Simulations and experiments on the ignition probability in turbulent premixed bluff-body flames

Michael Philip Sitte, Ellen Bach, James Kariuki, Hans-Jörg Bauer & Epaminondas Mastorakos

Published online: 18 Apr 2016.

Submit your article to this journal ⬈

View related articles ⬈

View Crossmark data ⬈

Full Terms & Conditions of access and use can be found at
http://www.tandfonline.com/action/journalInformation?journalCode=tctm20

Taylor & Francis
Taylor & Francis Group

Simulations and experiments on the ignition probability in turbulent premixed bluff-body flames

Michael Philip Sitte [a*], Ellen Bach[b], James Kariuki[a], Hans-Jörg Bauer[b] and Epaminondas Mastorakos [a]

[a]Department of Engineering, University of Cambridge, Cambridge, UK; [b]Institut für thermische Strömungsmaschinen, Karlsruhe Institute of Technology, Karlsruhe, Germany

The ignition characteristics of a premixed bluff-body burner under lean conditions were investigated experimentally and numerically with a physical model focusing on ignition probability. Visualisation of the flame with a 5 kHz OH* chemiluminescence camera confirmed that successful ignitions were those associated with the movement of the kernel upstream, consistent with previous work on non-premixed systems. Performing many separate ignition trials at the same spark position and flow conditions resulted in a quantification of the ignition probability P_{ign}, which was found to decrease with increasing distance downstream of the bluff body and a decrease in equivalence ratio. Flows corresponding to flames close to the blow-off limit could not be ignited, although such flames were stable if reached from a richer already ignited condition. A detailed comparison with the local Karlovitz number and the mean velocity showed that regions of high P_{ign} are associated with low Ka and negative bulk velocity (i.e. towards the bluff body), although a direct correlation was not possible. A modelling effort that takes convection and localised flame quenching into account by tracking stochastic virtual flame particles, previously validated for non-premixed and spray ignition, was used to estimate the ignition probability. The applicability of this approach to premixed flows was first evaluated by investigating the model's flame propagation mechanism in a uniform turbulence field, which showed that the model reproduces the bending behaviour of the S_T-versus-u' curve. Then ignition simulations of the bluff-body burner were carried out. The ignition probability map was computed and it was found that the model reproduces all main trends found in the experimental study.

Keywords: spark ignition; ignition probability; turbulent premixed flames; ignition modelling; bluff-body stabilised flames

1.   Introduction

Ignition of turbulent flames is very important for a wide range of propulsion applications [1,2]. In recent years, new insights have been developed into the fundamentals of spark ignition processes in non-premixed and spray systems [1,3]. In both experiments and modelling the key finding is that the kernels from the spark must grow and also be advected by the flow towards the anchoring points of the flame for the overall burner ignition to be successful. Therefore, apart from local processes that affect the success or not of the spark to develop a kernel, the long-term fate of the flame depends also on the convective pattern and on whether the flame may quench later, in other parts of the burner, as it propagates.

*Corresponding author. Email: mps59@cam.ac.uk

Large eddy simulations (LESs) have been shown to be a powerful tool for the simulation of spark ignition events [4–11]. However, due to the probabilistic nature of turbulent flows, repetitive simulations are required to assess the ignition characteristics including the ignition probability P_{ign} numerically [1]. In combination with LES, this approach leads to significant computational cost, in particular if several spark locations are to be tested. This shortcoming has motivated the development of physical models [12,13] based on the dominant factors found through experiment and detailed simulation. These low-order models significantly reduce the computational effort since they make use of a cold flow solution from computational fluid dynamics (CFD) instead of solving the transient ignition problem.

Spark ignition of turbulent premixed mixtures has been studied extensively [2,14] with emphasis on finding the conditions under which a kernel may be generated and propagate. A uniform mixture in isotropic homogeneous turbulence will lead to a flame if the spark has sufficient energy. The success or not of having subsequent flame propagation has been correlated with the Karlovitz number, Ka, which is the ratio of the flame time to the small-scale turbulence timescale [15,16]. Abdel-Gayed et al. [15] used

$$\text{Ka} = 0.157(u'/S_L)^2 \text{Re}_T^{-0.5}, \quad \text{Re}_T = u' L_T / \nu, \tag{1}$$

where u' is the magnitude of the characteristic turbulent velocity fluctuation, S_L the laminar flame speed, L_T the integral length scale and Re_T the turbulent Reynolds number. Ignition of the uniform mixture with a uniform turbulence field, as typically found in an explosion bomb experiment, will occur if Ka is below a critical value. In contrast to this relatively extensively-studied topic, the spark ignition of premixed burners has been studied very little.

The main differences between ignition of a mixture and the overall ignition of the burner are (i) that the latter involves the convection pattern in the (virtually always) re-circulating flow, which has been shown to be crucial for the ignition of non-premixed and spray systems [1,12] and also premixed burners [17,18], and (ii) the stabilisation of the flame, which is a burner-scale phenomenon and could potentially be understood by considering the blow-off behaviour of the burner. A swirling premixed flame has been ignited at various locations by a laser spark [17] and it was found that the locations giving successful ignition did not correlate with the local turbulence intensity, suggesting that more factors are at play. In contrast, ignition experiments on a confined premixed bluff-body flame found a negative effect of turbulent intensity and the ignition probability only for flow conditions close to extinction, but not for a case far from the lean stability limit [18]. Therefore, it is important to examine in detail whether there is a direct connection between the local Ka, the local mean velocity, and the statistics of ignition of a premixed burner.

The first part of this work consists of an experimental study examining the spark ignition of single bluff-body premixed flames. Moreover, it is attempted to correlate the regions of high ignition probability with the local Karlovitz number and velocity field, estimated based on previously-performed velocity measurements in the same burner [19]. The second part focuses on the modelling of the experimentally studied ignition process. The modelling effort follows the approach that was introduced by Neophytou et al. [12] for non-premixed flows. The applicability of an adapted version of this model to premixed flows is examined first, then simulation results for the experimentally-studied bluff-body burner are computed.
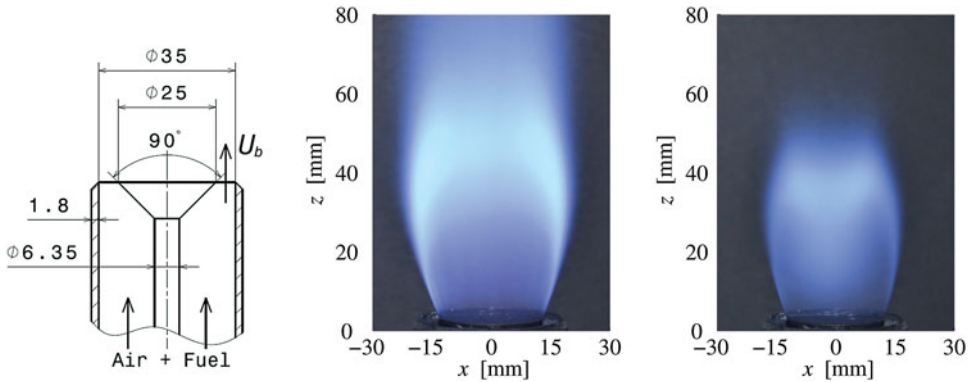
Figure 1.   CAD drawing of the bluff-body burner (left) and photographs of the ignited flames A1 (middle) and A4 (right). Note that flame A4 cannot be ignited by a spark, although it can be reached by altering the flow rates from A3. Photos reprinted from Combustion and Flame, Kariuki et al. [19], with permission from Elsevier.

2.   Methodology

2.1.   *Experimental set-up*

The bluff-body burner is shown in Figure 1 and is described in detail in [19]. It consists of a 25 mm bluff body placed in a 35 mm pipe open to the atmosphere. Air and gas are fully premixed upstream of the burner and their flow rates are controlled by mass flow controllers. Kariuki et al. [19] studied flames at various equivalence ratios with particle image velocimentry (PIV) and OH planar laser induced fluorescence (PLIF) from the point of view of blow-off limits and structure of the flame at various conditions approaching blow-off; here, the ignition behaviour at the same flow conditions is explored.

The electrical spark system has been used before [20,21]. Tungsten electrodes of 1 mm diameter with pointed ends were placed with a 2 mm gap in various locations across the flow. The electrical unit deposited very repeatable sparks [20] of duration 0.4 ms and energy 140 mJ . This is much higher than the minimum ignition energy, which is below 2 mJ in a methane–air mixture of equivalence ratio $\phi = 0.64$ [22].

Fast imaging (5 kHz) of OH^* chemiluminescence was used to image the ignition transient. A LaVision^{TM} IRO high-speed two stage intensifier with a spectral range of 190 to 800 nm was coupled to a Photron^{TM} SA1.1 monochrome high speed CMOS camera with 1024×1024 pixel resolution up to 5.4 kHz. This was fitted with a UV bandpass filter (270–370 nm) and the intensifier gated at 190 μs at 5 kHz. To protect the intensifier from the possibility of intense emission from the spark, the acquisition commenced once the spark had ended.

The PIV data of the cold (unignited) flow were from Kariuki et al. [19], from which the mean and RMS axial and radial velocities and the integral length scale of the turbulence were extracted. For each mixture, the Karlovitz number Ka was computed according to Equation (1). The magnitude of the characteristic turbulent velocity fluctuation u' for a three-dimensional velocity field can be defined by $3u'^2/2 = 1/2(u_{RMS}^2 + v_{RMS}^2 + w_{RMS}^2)$, where u_{RMS}, v_{RMS} and w_{RMS} are the RMS velocity fluctuations in the axial, radial and tangential directions, respectively. From the two-dimensional PIV data, u' is estimated as $[(u_{RMS}^2 + 2v_{RMS}^2)/3]^{1/2}$, assuming $w_{RMS}^2 = v_{RMS}^2$. The length scale L_T was found to be about 3 mm, not varying much at various locations, and so for the purposes of estimating

Table 1 Summary of experimental conditions for the bluff-body burner. U_b refers to the bulk velocity at the annulus (open area) of the burner.

Flame	U_b [m/s]	ϕ	Spark location (z/d, r/d)
A1	21.6	0.75	(0.5–1.25, 0.0–0.75)
A2	21.5	0.70	(0.5–1.25, 0.0–0.75)
A3	21.4	0.67	(0.5–1.25, 0.0–0.75)
A4	21.4	0.64	Cannot be ignited

the Karlovitz number later it was taken as uniform everywhere in the flow. The laminar flame properties needed in the definition of Ka were taken from laminar flame numerical solutions [19].

The ignition probability P_{ign} in the single-burner experiments was measured by performing 20 individual spark events and monitoring the number of overall flame ignitions achieved. Hence, the standard error of the mean for the ignition probability is $[P_{\text{ign}}(1 - P_{\text{ign}})/n]^{1/2} = 11\%$ if $P_{\text{ign}} = 50\%$.

The flow conditions are given in Table 1. The spark location is given in cylindrical coordinates (z, r), normalised with the bluff-body diameter $d = 25$ mm, where $z = 0$ on the surface of the bluff body. All the flames have the same air flow but decreasing equivalence ratio from flame A1 to flame A4. The bulk velocity changed very little due to the dominance of the air flow. The steady flames associated with these conditions have been examined by Kariuki et al. [19] in terms of their structure. Flame A1 is considered far from extinction, while flame A4 is very close to the blow-off point. Therefore, in contrast to the experiments of Cordier et al. [17], which were done with a premixed burner far from the blow-off point, here we also try to ignite flames far from and very close to the blow-off point.

2.2. *Low-order modelling*

The low-order ignition model SPINTHIR was employed to simulate the transient ignition process. This stochastic model had been introduced by Neophytou et al. [12] to assess ignition probability for non-premixed and spray burners. This model was adapted here for the ignition of a premixed flow. Its features are as follows.

The model simulates the flame propagation as the motion of virtual *flame particles*, using a random walk to mimic the effect of turbulent mixing. A time-averaged cold flow CFD solution and the laminar flame speed as a function of equivalence ratio are the only required inputs to simulate ignition events for an arbitrary spark position. The approximation of using a cold flow solution throughout the ignition process will be discussed later.

The algorithm is set up as a cellular automaton model, i.e. the cells of a grid change their status according to a well-defined set of rules. The fluid domain is filled with a coarse rectangular grid. Each grid cell has only two possible states: cold and burnt. At the beginning all cells are cold. A spark is simulated by switching the cells in the spark volume from cold to burnt. When a cell switches its state from cold to burnt, it emits one single virtual flame particle which follows a random walk. Whenever a flame particle enters a cold cell, then this cell is switched to the burnt state and emits one additional flame particle. The fraction of burnt cells relative to the total number of flammable cells, denoted by the ignition progress factor π_{ign}, is used to monitor an ignition event. In order to decide upon the success of a spark event, Neophytou et al. [12] proposed a criterion based on this value, where successful ignition corresponds to a π_{ign} above a certain threshold $\pi_{\text{ign, crit}}$. A burnt cell cannot be

switched back to its original cold state. This choice makes π_{ign} an unambiguous metric for the burner volume that has been visited by the cloud of flame particles. While this irreversibility caps the maximum number of particles in one simulation, it is without any further consequences on the evolution of the particle cloud, since the particles once emitted do not interact with the cells any more (see below). As such the cells' state constitutes an abstract measure of the ignition progress, which does not coincide with the position of the flame.

The ignition process is driven by the virtual flame particles. These particles are emitted by the cells and follow a random walk until being quenched by strong turbulence. Hence, the random walk mimics the motion of a small kernel in the turbulent flow field. Moreover, the cloud of particles grows as additional ones are emitted by the cells. In Section 3.2.1, the evolution of the particle cloud is investigated in terms of its capability to reproduce features of flame growth and propagation.

The random walk is given by a simplified Langevin model described by Equations (2) and (3), where $\Delta\mathbf{X}_p$ denotes the displacement vector of a particle p during the time interval Δt and its respective velocity is $\mathbf{U}_p$. $C_0 = 2$ is a constant and $\mathbf{N}_p$ a vector with a random direction whose length follows a Gaussian distribution $\mathcal{N}(0, 1)$. The other parameters are taken from the cold flow CFD solution. Here, L_T is the integral length scale and u' the turbulent velocity fluctuation estimated as $\sqrt{k}$, where k is the turbulent kinetic energy; $\widetilde{\mathbf{u}}$ is the local Favre averaged velocity and ε the local turbulent dissipation rate. Note that this model does not consider the effects of molecular diffusion or gas expansion.

$$\Delta\mathbf{X}_p = \mathbf{U}_p\Delta t \tag{2}$$

$$\Delta\mathbf{U}_p = -\left(\frac{1}{2} + \frac{3}{4}C_0\right)\left(\frac{L_T}{u'}\right)(\mathbf{U}_p - \widetilde{\mathbf{u}})\Delta t + (C_0\varepsilon\Delta t)^{1/2}\mathbf{N}_p. \tag{3}$$

Additionally, an extinction criterion is applied to decide whether a flame particle remains active or extinguishes. This flame quenching criterion is based on the Karlovitz number as introduced by Abdel-Gayed and Bradley [23]. For each flame particle the Karlovitz number is calculated in every time step according to Equation (1). In the original model for a non-premixed flow [12] L_T, $u' \sim \sqrt{k}$ are taken from the cold flow CFD solution and an equation is solved for the mixture fraction of a flame particle ξ_p, which is required for the computation of $S_L(\xi_p)$. The flame particle extinguishes if Ka_p exceeds the critical value $\mathrm{Ka}_{\mathrm{crit}} = 1.5$.

This model was adapted for premixed burners and two modifications were introduced, the most important being a randomisation of the Karlovitz number. In the original model [12], a locally constant value $u'(\mathbf{x})$ from the cold flow CFD solution was used to compute Ka_p. Of course, in the non-premixed case, the availability of fuel most prominently determines the survival of a kernel and the probabilistic nature of local flame quenching was due to random fluctuations of the mixture fraction. On the other hand, in a premixed flow this means that all flame particles passing through the same flow region experience the same u' resulting in the same Ka_p. Instead of using the locally constant u' from CFD in the present premixed case, the Karlovitz criterion now uses the turbulent fluctuation that the particle is actually experiencing through the random walk. In other words, the particle's Karlovitz number is higher if its motion is characterised by strong velocity fluctuations. Hence, the parts of the flame exposed to violent turbulence are more likely to extinguish. The second modification of the model is an extension to account for the case of flame–wall

contact. Considering initially cold walls of the combustion chamber, all flame particles are extinguished if they enter into contact with a wall. Hence the position of all active flame particles is tested after every step of the random walk. Those particles that are suddenly found outside the domain have either left through an open surface with an outlet boundary condition or a wall. In the latter case they are considered to be quenched by wall contact and are, thus, switched to the extinguished state.

Neophytou et al. [12] proposed guidelines for the time step and the grid size. These suggestions are based on necessity to assure consistency with the random walk and the Karlovitz criterion from a statistical point of view. Consequently, the time step $\Delta t < L_T/u'$ and the grid spacing $18\eta_K < \Delta x \leq 2(C_0 \varepsilon \Delta t)^{1/2} \Delta t$, where η_K is the Kolmogorov scale, can be retained when the model is used for premixed flows. The spatial discretisation is discussed thoroughly in the appendix of [12], concluding that grid dependence is small if the above-mentioned limits are respected.

2.3. *Cold flow CFD solution*

The cold flow field was computed with a steady-state Reynolds-averaged Navier-Stokes (RANS) simulation using the commercial CFD software ANSYS Fluent®. The turbulence model used was a realisable k–ε model with standard parameters. The computational domain had a cylindrical shape of diameter 200 mm and height 200 mm with an inflow boundary condition at the level of the annulus between bluff body and pipe. The velocity and turbulent intensity at the inlet were fixed according to experimental data [19]. Moreover, the mixture fraction at the inlet was fixed at the value $\xi = \phi/(\phi + [1 - \xi_{st}]/\xi_{st})$, corresponding to the the equivalence ratio ϕ indicated in Table 1, while $\xi_{st} = 0.055$ is the stoichiometric mixture fraction. Zero-gradient boundary conditions for the velocity and the mixture fraction as well as constant pressure were set at the outlet surface. A far-field condition was applied at the boundaries to the ambient air at the bottom and the sides of the domain with zero gradient velocity and pressure as well as fixed mixture fraction $\xi = 0$. The surface of the bluff body was modelled as a wall with a no-slip boundary condition. The domain was meshed with an unstructured tetrahedral grid with 130k nodes. The grid was refined in the region of the recirculation zone and around the inlet, where the grid size was 1.5 mm.

For the use of the cold flow field by the ignition model, the CFD solution was interpolated on a regular grid (grid spacing 2 mm) in a cubic domain with an edge length of 100 mm. The edges of this domain are indicated in Figures 11, 12 and 13.

3. Results and discussion

3.1. *Experiments*

3.1.1. *Ignition visualisation*

Photographs of the ignited premixed flame at conditions A1 and A4 are shown in Figure 1. Flame A4 is very close to the blow-off point (at this velocity, blow off occurs at an equivalence ratio 0.63), while flames A3 to A1 are progressively farther from the blow-off condition.

A sequence of a successful ignition event for flame A1 from spark position $(z/d, r/d) =$ (1, 0.4) is shown in Figure 2. It is evident that the kernel has moved off the spark in the upstream direction and eventually grows to ignite the full flame. At times during the flame evolution, the flamelet may be small, but even a small flame surviving upstream will be enough to ignite the burner. Similar evolutions are observed from other locations
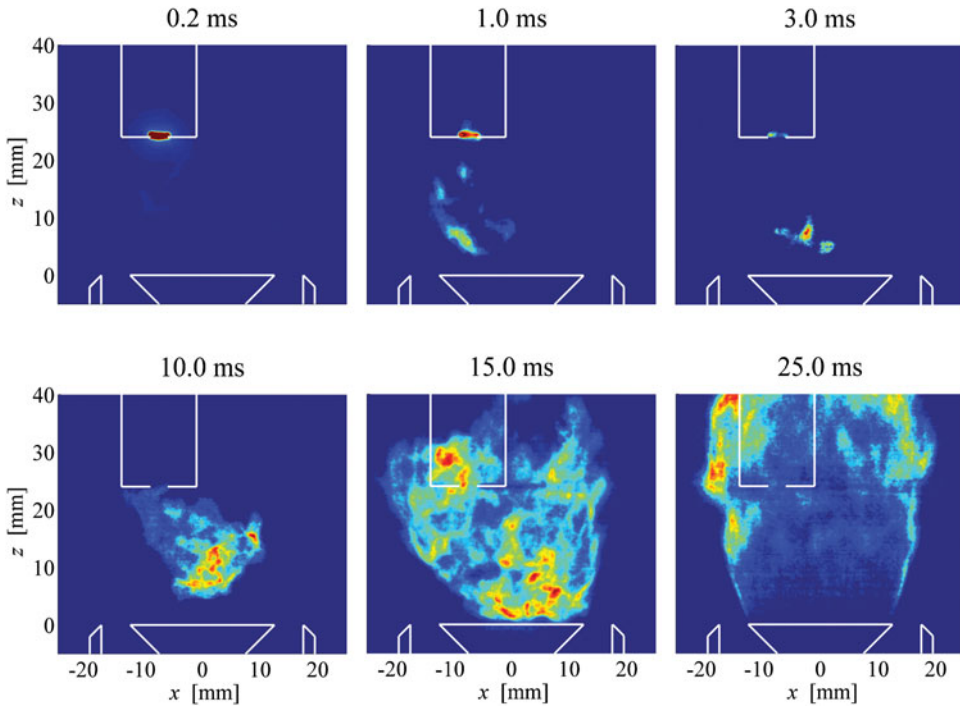
Figure 2. Evolution of a successful flame from a spark at (z/d, r/d) = (1, 0.4) for flame A1. Visualisation by 5 kHz OH* chemiluminescence. The times given are from the end of the spark.

with negative velocity. From locations with positive axial velocity, the kernel may get convected downstream, but if the flame grows enough in the radial direction to get inside the recirculation zone, then the flame has a good chance of growing fully. The movement of the flame upstream is key to successful ignition, consistent with previous work with non-premixed [21] and spray [3] laboratory flames and single-sector gas turbine combustors [24,25].

From sequences such as those in Figure 2, the time needed to achieve full flame ignition has been evaluated by examining the time instant when the integrated light emission stabilises. The time to establish a stable flame for the whole burner did not depend significantly on the ignitor location. The main finding was that, as we progress from flames A1 to A3, the time needed to ignite was longer. For example, with ignition along the axis at (z/d, r/d) = (1, 0), flame A1 takes approximately 20 ms, while flame A3 takes about 100 ms. This is likely to be partly due to the laminar flame speed difference between these two equivalence ratios (0.24 versus 0.17 ms) and partly because the flow condition approaches the blow-off condition, which increases the probability of localised quenching, which in turns slows down the overall ignition of the burner.

3.1.2.   *Ignition probability*

In order to understand better the following discussion on the ignition probability, the mean axial velocity is presented in Figure 3. The recirculation zone (RZ) extends downstream about one bluff-body diameter and the radial location of maximum axial velocity (annular
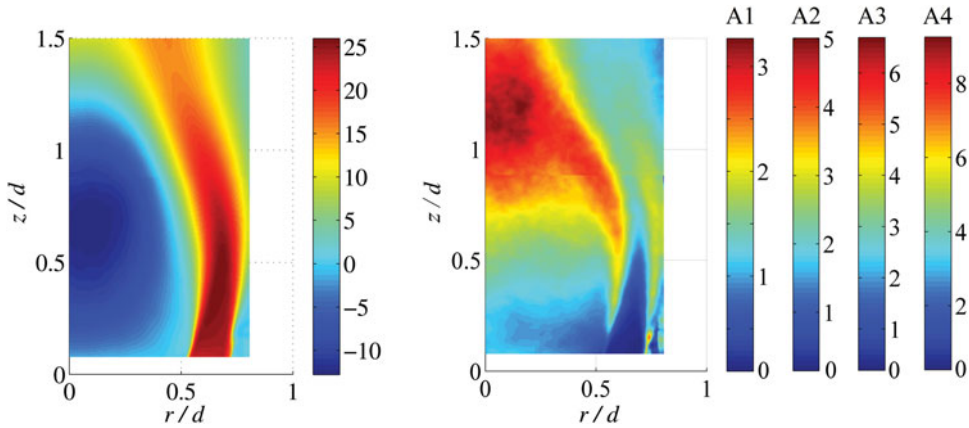
Figure 3. The mean axial velocity in m/s (left) and the Karlovitz number (right) based on the cold flow PIV measurements [19].
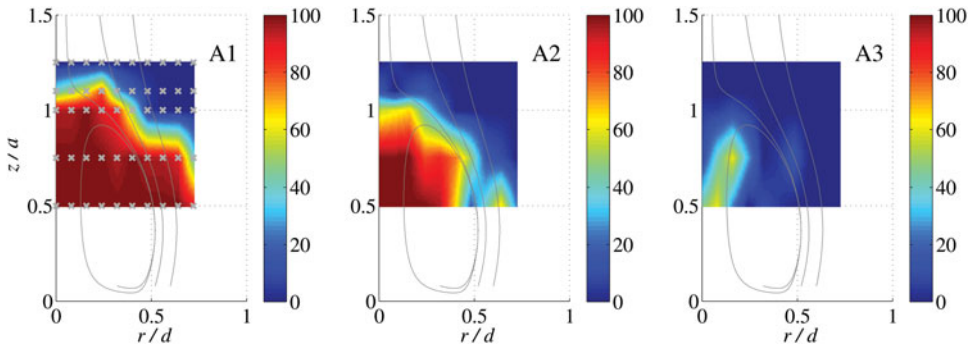

Figure 4. Ignition probability maps (P_{ign}%) for cases A1 (left), A2 (middle) and A3 (right). The grey ×-markers on the left map indicate the spark positions tested experimentally. Streamlines computed from the CFD solution will be presented later.

jet) is at about $r/d = 0.7$ for $z/d = 0.5$ and $z/d = 0.75$, shifting inwards further downstream. The thickness of the RZ is about $0.5d$ up to these locations.

Surface plots of the measured P_{ign} for the flames A1–A3 are shown in Figure 4, while the discrete spark positions tested are marked on one probability map. It is evident that the ignition probability has very large spatial variations and that it changes very significantly with the equivalence ratio of the flame. First, at large radii, P_{ign} approaches zero for all axial locations, which is partly due to the ambient air entrainment. However, even in locations inside the recirculation zone, only flame A1 has $P_{ign} = 1$. Second, flames A2 and A3 have, progressively, smaller P_{ign} than flame A1 at all radial and axial locations. Even in the centre of the RZ, flame A3 has very low ignition probability. Finally, as we go downstream, a sudden drop in P_{ign} is visible. Observation with the camera suggests that sparking in these locations produces kernels, but these kernels are convected away, presumably because of the positive mean velocity in these locations.

Flame A4 is stable, but can be reached only by igniting a richer flame and then adjusting the flowrates; A4 cannot be ignited by the present spark ($P_{ign} = 0$ everywhere). This demonstrates a well-known characteristic of gas turbine combustors: the so-called 'ignition
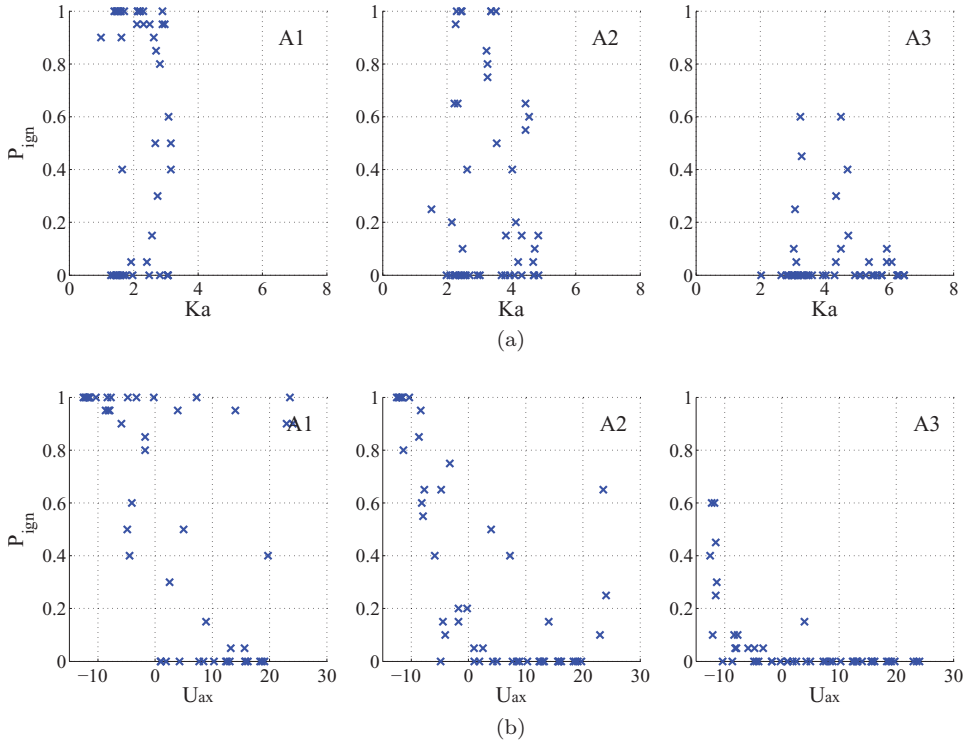
3

When one plots the $P_{\rm ign}$ from every spark location versus the mean axial velocity at the same location, a trend that $P_{\rm ign}$ increases when the velocity is negative becomes evident (Figure 5). Only flame A1 (the richest one examined here) can be ignited with high $P_{\rm ign}$ in some regions with positive axial velocity.

It is clear therefore that successful ignition events arise, in a statistical sense, from flow conditions and spark locations that not only have low Ka, but also negative axial velocity, so that the kernels not only survive unquenched, but are also convected towards the bluff body. This is in perfect agreement with the discussion and review of experimental data from non-premixed and spray burners in Neophytou et al. [12]. The present data emphasise further the effect of mean convection and local turbulence on the ignition of burners. They also suggest that to be able to capture ignition transients properly with LES, the combustion model must include local quenching. This seems to be included in some efforts [6–8], but further validation is necessary and the present data can be used for that purpose.

3.2. *Ignition modelling*

3.2.1. *Prediction of the turbulent burning velocity*

Experimental findings showed that local flow quantities may not be sufficient to judge the ignitability of a burner and underlined the importance of convection of the initial kernel also being exposed to localised extinction. These key features are included in a simplified physical model that was proposed by Neophytou et al. [12] for the ignition of non-premixed flows. Whereas this model was successfully applied to the ignition of non-premixed and spray flames, the approach has not yet been used to simulate the ignition of a premixed flame.

To assess the applicability of the model to premixed flows, its flame propagation mechanism is investigated. The turbulent burning velocity S_T is chosen as the key quantity to judge the quality of this feature and the following test is performed. The ignition model's *virtual* burning velocity is defined over the time the flame particles take to cross a given distance. In order to determine this quantity, the model is used on an elongated domain with square cross section, filled with a uniform air–fuel mixture. In the absence of a mean flow, the velocity field is given by non-decaying, uniform, isotropic turbulence. The domain is at least $2L_T$ wide and $10L_T$ long to limit boundary effects. In addition, the flame–wall interaction is changed and incoming flame particles are now reflected to cancel out effects of limited size. For the range of velocity fluctuations investigated, the grid size is set to $\Delta x = 2$ mm and the time step is 2 ms for $u' < 10$ m/s and 1 ms above.

Figure 6 shows a typical case of flame propagation after having initiated the ignition by switching all cells on one surface to the burnt state. At $t = 0$ ms all flame particles are active; at later times the majority is extinguished, with a few active ones driving the propagtion. In order to monitor the flame propagation, the ignition progress factor $\pi_{\rm ign}$ – the fraction of burnt cells in the domain evolving in time – is a useful indicator. It corresponds closely to the spatial expansion of the particle cloud but is more clearly defined. The graph is smooth and rises almost linearly for $70 < t < 120$ ms and the virtual mean turbulent burning velocity is calculated from the slope of $\pi_{\rm ign}$ in this interval of linear growth, as shown in Figure 6. $\pi_{\rm ign}$ does not reach 100% but nevertheless the flame particles successfully travel over the entire length of the domain. As u' increases, the number of cells that are ultimately visited by flame particles decreases until no flame particle manages to reach the opposite side of the domain, as shown in Figure 7. Due to the randomised Ka$_p$ the propagation initially starts, but eventually more existing flame particles extinguish than new ones are generated.
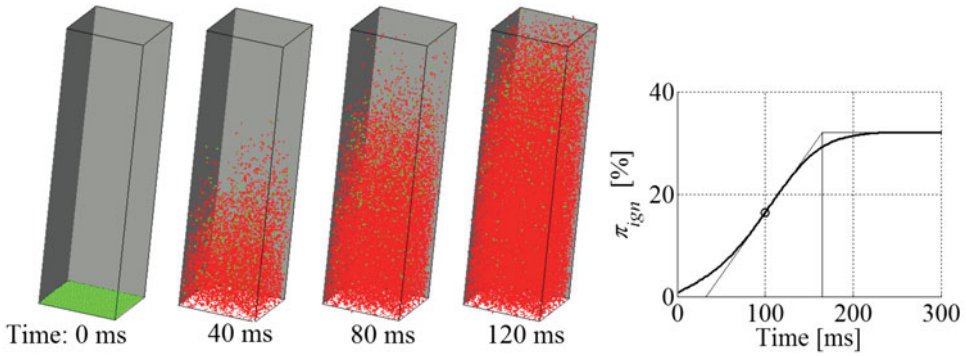
Figure 6.　　Successful flame propagation for $u' = 9$ m/s and $L_T = 30$ mm; particle tracking information (left) and π_{ign} (right).
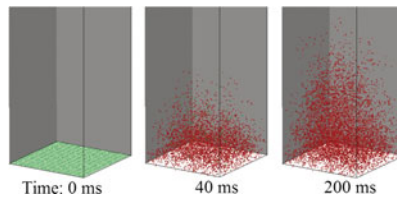

Figure 7.　　Failed flame propagation for $u' = 10$ m/s and $L_T = 30$ mm.

The results for the virtual burning velocity, simulated with an equivalence ratio $\phi = 0.7$ and non-dimensionalised with S_L are compared to experimental data in Figure 8. M 1 represents the model's virtual burning velocity for a constant large-eddy length scale $L_T = 30$ mm and SWL 00 are experimental results by Shy et al. [26]. In a second step, the model is run for a variable turbulent length scale (M 2) taking $L_T = L_T(u')$, which
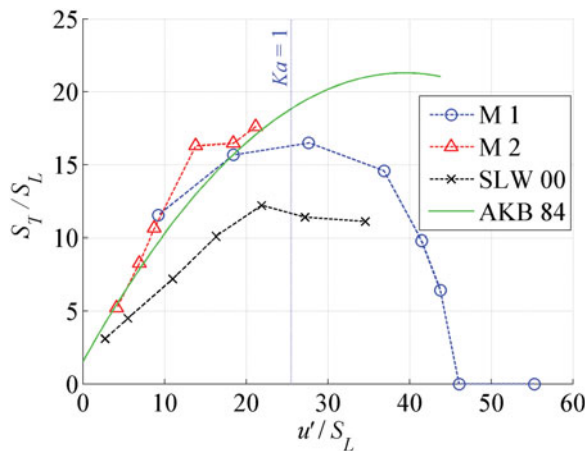

Figure 8.　　Mean turbulent burning velocity S_T. The model's virtual burning velocity for constant (M 1) and variable L_T (M 2) is compared to experimental results by Shy et al. [26] (SWL 00) and Abdel-Gayed et al. [15] (AKB 84).

corresponds to the measurements by Shy et al. [26]. AKB 84 is a quadratic fit to experimental results by Abdel-Gayed et al. [15].

Primarily, one notes that M 1 and M 2 are very similar even though in the latter L_T varies from 10 mm for $u' \approx 1$ m/s to 50 mm for ≈ 4.5 m/s. This shows that, as far as the ignition model is concerned, the influence of the turbulent length scale is small. Apparently, M 1 (constant L_T) is a good indicator for the general behaviour of the model.

Secondly, the model's virtual burning velocity shows the same characteristics as the experiment (SWL 00). For a low turbulent intensity, S_T/S_L increases steadily, but for larger u' the slope becomes progressively smaller. Eventually, a maximum turbulent burning velocity is reached, followed by a slow decrease until flame propagation is not possible any more due to excessive local quenching. In their experimental study, Shy et al. [26] described three regions: first, an abrupt increase of S_T/S_L for $u'/S_L \sim O(1)$ (region I); secondly, a region where the slope of the turbulent burning velocity is bent toward the horizontal (region II); and finally, a slight decrease of S_T/S_L for high values of u'/S_L (region III). It is notable that the ignition model used here is not applicable to flows characterised by region I. Since no mechanism of laminar flame propagation is built into it, the model can give reasonable results for $S_T/S_L \gg 1$ only. In region II, the turbulent burning velocity does not increase beyond $\approx 12 S_L$. Shy et al. suspected the change from the corrugated flamelet to the distributed regime as the reason. In contrast, the ignition model (M 1) is only based on localised quenching of the flame, one particular phenomenon which has surprisingly not been reported for this experiment. However, quenching was observed by Abdel-Gayed et al. [27] at Karlovitz numbers above one, which for the data set M 1 is indicated by the dotted vertical line in Figure 8. Due to the stochastic approach followed in the model, the influence of flame quenching happens gradually and is preceded by a long decay of S_T/S_L.

Finally, the simulated results for S_T (M 1 and M 2) are larger than the corresponding experimental ones. However, different empirical studies on the turbulent burning velocity also differ by significant amounts. For instance, measurements by Bradley [28] are larger than SLW 00 by a factor of ≈ 2. A good indicator for this is AKB 84 by Abdel-Gayed et al. [15], which corresponds well to the simulated results. We conclude from this numerical experiment that the ignition model is capable of mimicking some key trends of turbulent flame propagation, which suggests that the model can be used for ignition simulations of turbulent premixed flames.

3.2.2. *Application to the bluff-body burner*

In the previous section, the ignition model's capability to reproduce the correct turbulent burning velocity in a premixed flow was tested. The model is now applied to the premixed bluff-body burner. The grid size is $\Delta x = 2$ mm and the time step is $\Delta t = 0.5$ ms. The spark volume is estimated based on the images from the experiment.

Figure 9 shows the mean velocity and mean mixture fraction for the flame A1, where $\xi = 1$ corresponds to pure fuel. Inside the recirculation zone (RZ) the average fuel–air ratio is almost uniform and ξ does not decrease by more than 2% along the symmetry axis within two bluff-body diameters downstream from the inlet. The radial profiles of the mean axial velocity from experiment and simulation are compared in Figure 10. The profiles are shown for three axial locations correspond to the dashed lines in Figure 9. The CFD results are smoother and the size of the RZ is slightly underpredicted but, in general, the convective pattern of the burner as well as the minimum and maximum velocity are captured reasonably well for this application.
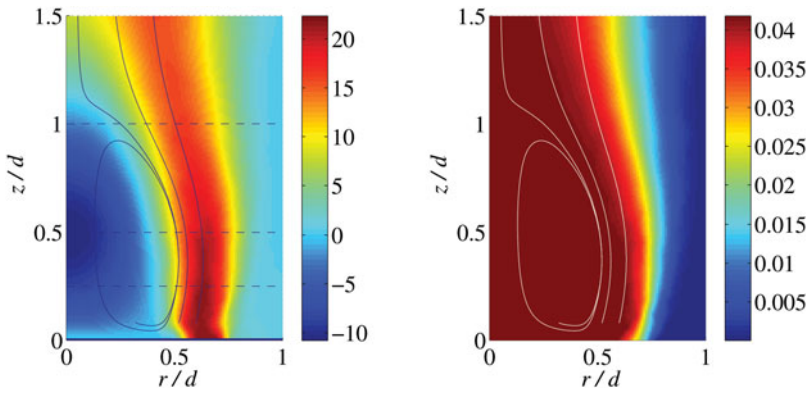
Figure 9.   Cold flow CFD solution: mean axial velocity U_{ax} m/s (left) and the mean mixture fraction ξ (right) where $\xi = 1$ corresponds to pure fuel. Note: The flammability limits of a methane–air mixture are $\xi_{lean} = 0.028$, $\xi_{rich} = 0.089$ and the stoichiometric mixture fraction is $\xi_{st} = 0.055$ [29].
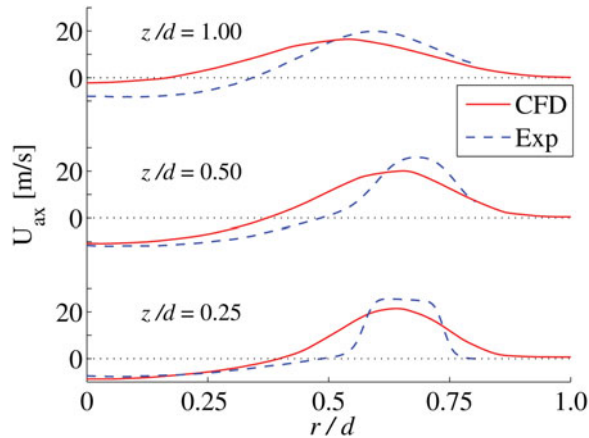

Figure 10.   Comparison of experimental PIV results (dashed lines) and RANS (continuous lines). Axial distance z/d corresponds to the dashed lines marked in Figure 9.

Several typical ignition pathways can be distinguished when simulating various ignition events, sparking in different locations. The typical case of a successful ignition event is shown in Figure 11. For an equivalence ratio of 0.75, the spark location is placed in the middle of the recirculation zone, 0.5 bluff-body diameters above the outlet. The contour plot shows the field of the Karlovitz number, calculated from mean flow quantities from the CFD solution (note that this is Ka based on $\sqrt{k}$, not Ka_p experienced by the individual flame particles). The kernel is convected upstream with the mean flow and some flame particles are quenched when getting in contact with the bluff body. However, the rest are convected around the RZ and burn most of the flammable mixture. Figure 11 also shows a plot of the ignition progress factor, and the ignition pathways of 50 spark events are shown. The images shown at the left correspond to the dominant case where π_{ign} rises quickly and ultimately reaches 70%. Of course, the model cannot actually assess whether the flame is stabilised, but, as proposed by Neophytou et al. [12], we infer that a successful ignition
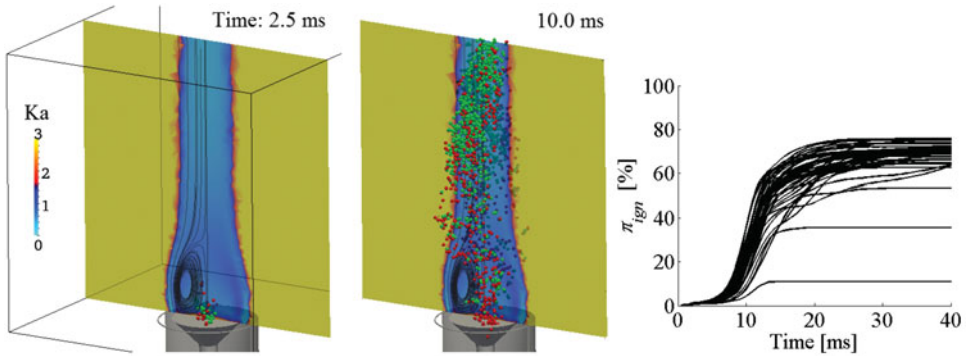
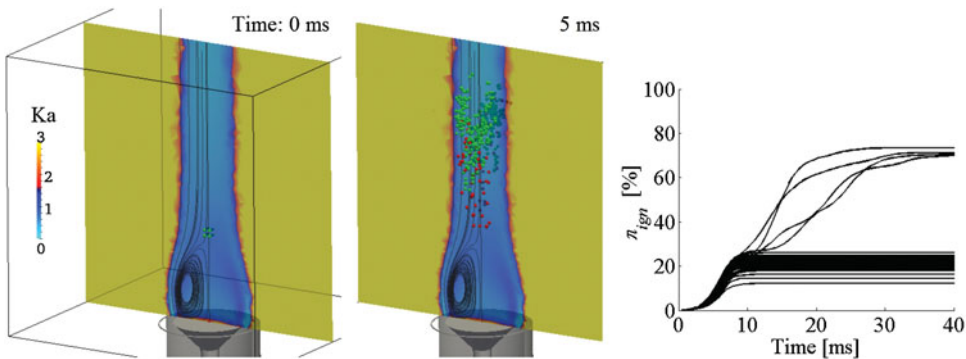Figure 11.   Successful ignition event of the single burner with $\phi = 0.75$.

Figure 12.   Ignition failure after sparking downstream of the recirculation zone for $\phi = 0.75$.

corresponds to a value of π_{ign} above a certain threshold. In this case, it seems reasonable to speak of a successful ignition since most of the flammable mixture is burned. Furthermore, active flame particles enter the RZ and burn most cells at its inside. The associated heat release would warm up fresh gases, a mechanism which is believed to be critical for flame stabilisation [21].

In contrast, sparking downstream of the RZ most likely causes an ignition failure, as shown in Figure 12. In this case, the flame particles are convected downstream and the RZ remains untouched. This event corresponds to the large majority of cases shown in the π_{ign} plot, where only a small fraction of flammable mixture is burned. Yet the ignition pathways show that only rarely (4 events in 50) is the kernel caught by the RZ, which results in a successful ignition such as described earlier. Finally, Figure 13 shows that for a very fuel-lean case the kernel extinguishes even if the spark location is in the centre of the RZ. This is due to a very high Karlovitz number in some parts of the RZ as can be seen in the integrated contour plot. In this case, the flame is quenched in zones of strong shear and by contact with the bluff-body surface.

These qualitative investigations finally allow comments to be made on the modelling choice of using a cold flow solution throughout the ignition event. Generally, this approximation supposedly holds at the beginning of an ignition event, while gradually losing its accuracy as the flame grows bigger. However, the advection of a small kernel in this first stage seems to be most critical and all ignition failures observed occur before large amounts
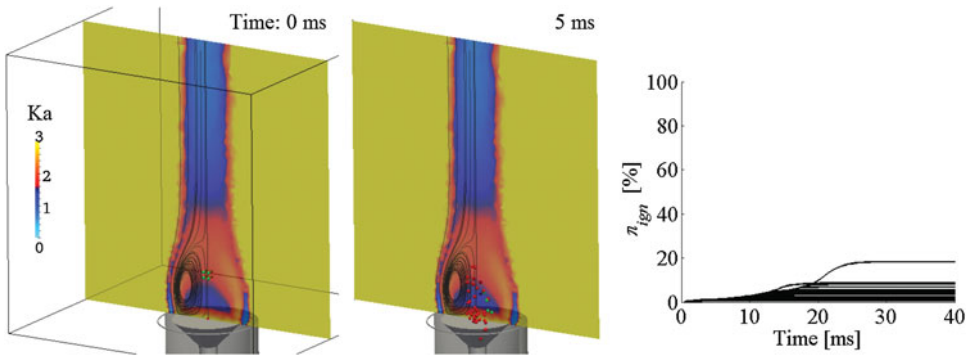
Figure 13.   Ignition failure for $\phi = 0.64$. (colour online)

of gas are burnt. Conversely, the heat release from burning large gas volumes would support a further growth of the flame, leading to complete ignition. Thus, the approximation seems reasonable since the model's predictions of ignition success or failure are interpreted in a statistical sense through the ignition probability.

Comparing the pathways of successful ignition in Figures 11 and 12 shows that the flame A1 takes between 20 and 30 ms until π_{ign} reaching its final value, independent of the spark location. While these results agree well with the time of ignition for the flame A1 found in experiments, we don't find that this time increases for leaner cases. In fact, the flames A2 and A3 take just as long as A1 to reach the final value of π_{ign} (not shown). This time is dominated by the residence time of flame particles in the RZ, which is limited, however, by the fact that every cell can only emit one flame particle when it is irreversibly switched to the burnt state. Here we recall that the model simulates the growth of an initial kernel, while it cannot assess the time necessary for the stabilisation of the flame.

The ignition probability map is computed next by simulating 100 spark events for a whole set of locations with a 2 mm spacing in the radial and axial directions. A spark is assumed to ignite the burner if $\pi_{ign} > \pi_{ign, crit}$. Following the procedure previously employed by Neophytou et al. [12], $\pi_{ign, crit}$ is determined from the ignition pathways and in particular the terminal value of π_{ign} of typical spark events, as shown in Figures 11, 12 and 13. In these cases, most spark events either reach $\pi_{ign} \approx 70\%$ or remain around 20%. Therefore setting the threshold $\pi_{ign, crit}$ to 30% or increasing it to 60% does change the resulting ignition probability significantly, which demonstrates a certain robustness of this criterion. Flames A2 and A3 are more sensitive to the threshold value than A1, but the general trends shown later are unchanged. Eventually, the threshold $\pi_{ign, crit} = 30\%$ is chosen – this is the least restrictive value that is still sufficient to rule out the clear ignition failures shown in Figures 12 and 13.

Surface plots of the ignition probability for the flames A1, A2 and A3 are shown in Figure 14; for A4, $P_{ign} = 0$ everywhere. Note that the ignition probability was simulated for a wider area than could be investigated experimentally. In particular, the numerical results include the region close to the bluff body where experiments could not be performed with the electric sparking system. The area investigated experimentally is indicated by a grey frame in Figure 14. The ignition model reproduces the following three key points from the experimental study.
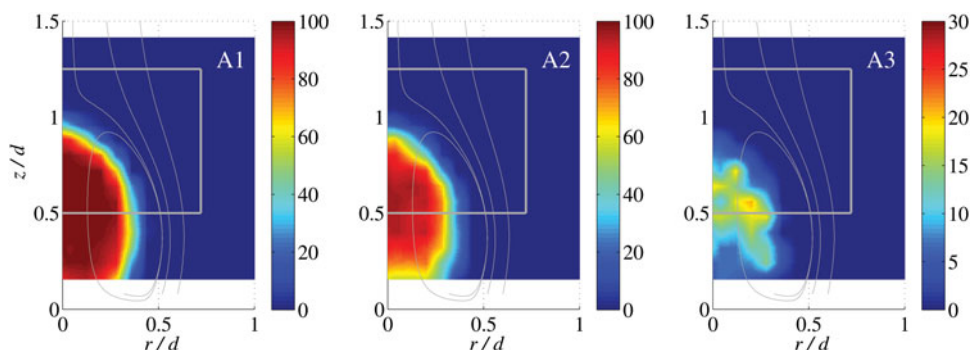
Figure 14. Ignition probability map (P_{ign} %) computed with the ignition model for flames A1, A2 and A3 (from left to right). The rectangle signifies the area investigated experimentally and shown in Figure 4. Streamlines shown are taken from the CFD solution.

- The ignition probability is high in the proximity of the axis, decreases in the radial direction, and approaches zero for large radii due to the scarcity of fuel as the annular jet mixes with ambient air.
- The ignition probability decreases in the axial direction and drops abruptly at the downstream end of the central recirculation zone since the initial kernel is convected downstream and fails to ignite the flammable mixture close to the bluff body.
- The burner is less likely to be ignited successfully if the fuel–air mixture is leaner. Hence P_{ign} decreases from $\phi = 0.75$ to 0.67, the leanest case $\phi = 0.64$ being impossible to ignite.

The reproduction of these main trends is considered adequate for the purpose of using the model for exploring the ignition behaviour of combustors. While the overall effect of decreasing ϕ on P_{ign} is not surprising, we note that the model managed to quantify this effect relatively well, considering that flame A3 was still ignitable whereas A4 was not. Furthermore, the experiments generally found a larger ignitable area, which can be partly explained by the underprediction of the length and width of the RZ by the RANS simulation. Moreover, the numerical results show that P_{ign} drops rapidly in the radial direction due to a scarcity of fuel, which results in a high Karlovitz number and immediate quenching. Conversely, Ahmed [18] observed a finite ignition probability even in some areas where no flammable mixture was present. A possible solution could be the introduction of a 'memory effect' into the model, in which the virtual flame particle is not immediately quenched upon meeting $Ka > Ka_{crit}$ regions, as suggested by Soworka et al. [30] following Richardson [31]. In addition to the trends found in the experiments, the ignition model also predicts the highest ignition probability for $z/d \approx 0.5$, while P_{ign} decreases closer to the bluff body. This behaviour is also seen in P_{ign} measurements of a premixed confined bluff-body burner studied by Ahmed [18]. Since turbulent velocity fluctuations, and hence the local Ka, are typically low in this area (Figure 3), we attribute this effect to the quenching of the initially small kernel after contact with the bluff body.

4. Conclusions

The ignition behaviour of a single bluff-body stabilised premixed burner has been examined experimentally and numerically. The probability of ignition P_{ign} has been measured

experimentally at various flow conditions and locations. It was found that sparking inside the recirculation zone maximised the likelihood of success, although P_{ign} decreased substantially as the flame became leaner. A direct comparison between the local P_{ign} and the estimated Karlovitz number Ka showed that, in general, P_{ign} was high where Ka was low, but an additional condition for high P_{ign} was that the mean velocity had to be negative (i.e. towards the bluff body). The time taken to ignite the flame increased as the equivalence ratio decreased. Flames very close to the blow-off condition could not be ignited by a spark, although they were reachable by igniting a richer flame and adjusting the equivalence ratio.

A stochastic low-order ignition model for non-premixed flows has been adapted to the present premixed case. Simulations on a rectangular domain and in the absence of mean flow were carried out to assess the model's capability of mimicking turbulent flame propagation. It was found that the model reproduced general trends of the mean turbulent burning velocity as a function of the velocity fluctuation including the 'bending behaviour' of S_T versus u', suggesting the model's applicability to the ignition process of premixed burners. Indeed, simulation results for the bluff-body burner globally match the findings from the experimental study and, in particular, good agreement is found for the influence of equivalence ratio and spark location on P_{ign}.

ORCID

Michael Philip Sitte http://orcid.org/0000-0002-7502-9858
Epaminondas Mastorakos http://orcid.org/0000-0001-8245-5188

References

[1] E. Mastorakos, *Ignition of turbulent non-premixed flames*, Prog. Energy Combust. Sci. 35 (2009), pp. 57–97.
[2] A.H. Lefebvre, *Gas Turbine Combustion*, 2nd ed., Taylor & Francis, London, 1999.
[3] T. Marchione, S.F. Ahmed, and E. Mastorakos, *Ignition of turbulent swirling n-heptane spray flames using single and multiple sparks*, Combust. Flame 156 (2009), pp. 166–180.
[4] M. Boileau, G. Staffelbach, B. Cuenot, T. Poinsot, and C. Bérat, *LES of an ignition sequence in a gas turbine engine*, Combust. Flame 154 (2008), pp. 2–22.
[5] G. Lacaze, E. Richardson, and T. Poinsot, *Large eddy simulation of spark ignition in a turbulent methane jet*, Combust. Flame 156 (2009), pp. 1993–2009.
[6] A. Triantafyllidis, E. Mastorakos, and R. Eggels, *Large eddy simulations of forced ignition of a non-premixed bluff-body methane flame with conditional moment closure*, Combust. Flame 156 (2009), pp. 2328–2345.
[7] W.P. Jones and A. Tyliszczak, *Large eddy simulation of spark ignition in a gas turbine combustor*, Flow Turbul. Combust. 85 (2010), pp. 711–734.

[8] V. Subramanian, P. Domingo, and L. Vervisch, *Large eddy simulation of forced ignition of an annular bluff-body burner*, Combust. Flame 157 (2010), pp. 579–601.

[9] W.P. Jones and V.N. Prasad, *LES-pdf simulation of a spark ignited turbulent methane jet*, Proc. Combust. Inst. 33 (2011), pp. 1355–1363.

[10] D. Barré, L. Esclapez, M. Cordier, E. Riber, B. Cuenot, G. Staffelbach, B. Renou, A. Vandel, L. Gicquel, and G. Cabot, Combust. Flame 161 (2014), pp. 2387–2405.

[11] M. Philip, M. Boileau, R. Vicquelin, E. Riber, T. Schmitt, B. Cuenot, D. Durox, and S. Candel, *Large eddy simulations of the ignition sequence of an annular multiple-injector combustor*, Proc. Combust. Inst. 35 (2015), pp. 3159–3166.

[12] A. Neophytou, E.S. Richardson, and E. Mastorakos, *Spark ignition of turbulent recirculating non-premixed gas and spray flames: A model for predicting ignition probability*, Combust. Flame 159 (2012), pp. 1503–1522.

[13] A. Eyssartier, B. Cuenot, L. Gicquel, and T. Poinsot, *Using LES to predict ignition sequences and ignition probability of turbulent two-phase flames*, Combust. Flame 160 (2013), pp. 1191–1207.

[14] D. Bradley and F.K.K. Lung, *Spark ignition and the early stages of turbulent flame propagation*, Combust. Flame 69 (1987), pp. 71–93.

[15] R.G. Abdel-Gayed, K.J. Al-Khishali, and D. Bradley, *Turbulent burning velocities and flame straining in explosions*, Proc. Roy. Soc. London A 391 (1984), pp. 393–414.

[16] D. Bradley, P. Gaskell, X. Gu, and A. Sedaghat, *Premixed flamelet modelling: Factors influencing the turbulent heat release rate source term and the turbulent burning velocity*, Combust. Flame 143 (2005), pp. 227–245.

[17] M. Cordier, A. Vandal, G. Cabot, B. Renou, and A. Boukhalfa, *Laser-induced spark ignition of premixed confined swirled flames*, Combust. Sci. Technol. 185 (2013), pp. 397–407.

[18] S.F. Ahmed, *The probabilistic nature of ignition of turbulent highly-strained lean premixed methane–air flames for low-emission engines*, Fuel 134 (2014), pp. 97–106.

[19] J. Kariuki, J.R. Dawson, and E. Mastorakos, *Measurements in turbulent premixed bluff body flames close to blow-off*, Combust. Flame 159 (2012), pp. 2589–2607.

[20] S.F. Ahmed and E. Mastorakos, *Spark ignition of lifted turbulent jet flames*, Combust. Flame 146 (2006), pp. 215–231.

[21] S.F. Ahmed, R. Balachandran, T. Marchione, and E. Mastorakos, *Spark ignition of turbulent nonpremixed bluff-body flames*, Combust. Flame 151 (2007), pp. 366–385.

[22] B. Lewis and G. von Elbe, *Combustion, Flames and Explosions of Gases*, 2nd ed., Academic Press, New York, 1961.

[23] R.G. Abdel-Gayed and D. Bradley, *Criteria for turbulent propagation limits of premixed flames*, Combust. Flame 62 (1985), pp. 61–68.

[24] R.W. Read, J.W. Rogerson, and S. Hochgreb, *Flame imaging of gas-turbine relight*, AIAA J. 48 (2010), pp. 1916–1927.

[25] A. Lang, R. Lecourt, and F. Giuliani, *Statistical evaluation of ignition phenomena in turbojet engines*, in *Proceedings of ASME Turbo Expo 2010: Power for Land, Sea and Air*, 14–18 June 2010, Glasgow, UK, Vol. 2, pp. 985–992.

[26] S. Shy, W.J. Lin, and J.C. Wei, *An experimental correlation of turbulent burning velocities for premixed turbulent methane–air combustion*, Proc. Roy. Soc. London A 456 (2000), pp. 1997–2019.

[27] R.G. Abdel-Gayed, D. Bradley, and M. Lawes, *Turbulent burning velocities: A general correlation in terms of straining rates*, Proc. Roy. Soc. London A 414 (1987), pp. 389–413.

[28] D. Bradley, *How fast can we burn?* Proc. Combust. Inst. 24 (1992), pp. 247–262.

[29] S.R. Turns, *An Introduction to Combustion: Concepts and Applications*, McGraw-Hill, London, 2000.

[30] T. Soworka, M. Gerendas, R. Eggels, and E. Mastorakos, *Numerical investigation on ignition performance of lean burn combustor at sub-atmospheric conditions*, in *Proceedings of ASME Turbo Expo 2014: Turbine Technical Conference and Exposition*, 16–20 June 2014, Düsseldorf, Germany. Vol. 4A, V04AT04A046 15pp.

[31] E.S. Richardson, *Ignition modelling for turbulent non-premixed flows*, Ph.D. thesis, University of Cambridge, 2007.